Amsterdam, The Netherlands: Excerptia Medica Found., pp. 429–436, 1966.
[31] C. A. Nugent, H. R. Warner, V. L. Estergreen, and K. B. Eik-nes, "The distribution and disposal of cortisol in humans," in *Proc. 2nd Int. Cong. Endocrinology, Pt. 1*, S. Taylor Ed. Amsterdam, The Netherlands: Excertia Medica Found., pp. 257–261, 1964.
[32] A. Kawai and F. E. Yates, "Interference with feedback inhibition of adrenocorticotropin release by protein binding of corticosterone," *Endocrinology*, vol. 79, pp. 1040–1046, Dec. 1966.
[33] N. Keller, L. R. Sendelbeck, R. I. Richardson, C. Moore, and F. E. Yates, "Protein binding of corticosteroids in undiluted rat plasma," *Endocrinology*, vol. 79, pp. 884–906, Nov. 1966.
[34] J. C. Porter, A. P. S. Dhariwal, and S. M. McCann, "Response of the anterior pituitary adrenocortical axis to purified CRF," *Endocrinology*, vol. 80, pp. 679–688, Apr. 1967.
[35] J. H. Milsum, *Biological Control Systems Analysis*. New York: McGraw-Hill, 1966.
[36] M. T. Jones and M. A. Stockham, "The effect of previous stimulation of the adrenal cortex by adrenocorticotrophin on the function of the pituitary-adrenocortical axis in response to stress," *J. Physiol.*, vol. 184, pp. 741–750, June 1956.

TOMOSYNTHESIS: A Three-Dimensional Radiographic Imaging Technique

DAVID G. GRANT

***Abstract*—A three-dimensional radiographic imaging system has been developed, and is presently being clinically evaluated. Twenty conventional radiographs are reduced and reprojected into a display volume according to a geometry which matches the X-ray source geometry. The images are integrated on a viewing screen and produce the tomographic plane corresponding to the screen's position. Planes parallel and tilted with respect to the scanning plane can be observed by simply adjusting the screen. The image is continuous in all directions, possesses a resolution of about 2*lp*/mm, and is usually true-sized, although factors of 2 or 3 in magnification can be easily produced.**

The patient dosage resulting from this technique is approximately the same as conventional tomography, but may be less by a factor of 2 or 3 for low-resolution situations.

This paper contains a brief theoretical summary, a description of image recording and projection apparatus, and typical results.

I. Summary

THE ABILITY of radiologists to visualize structures in a conventional radiography is determined by a number of physical factors. Perhaps the most important of these is the differential attenuation between the structure of interest and the surrounding volume. To a first approximation, this quantity determines the image contrast observed in the radiograph and provides the radiologist with more information than any other factor. There are a number of effects associated with all radiological systems which tend to obscure differential attenuation profiles. X-ray scattering, for example, reduces contrast by raising the overall background level of radiation. However, this problem has been minimized, or at least accommodated, to a satisfactory degree by a variety of techniques. Image degradation produced by shadows of intervening structures is another serious problem. Its solution was effected, at least partially, with the development of "body-section radiography" techniques (tomography). The basic principles of tomography were formulated by Ziedses des Plantes, starting in 1932 [1]. His work, and variations thereon, form the basis for almost all body-section radiography in use today. These techniques have proven quite successful, and are frequently used in hospitals and clinics throughout the country.

Tomographic systems are designed to produce images by a process which preserves the differential attenuation profile of a planar cross section. Variations in the basic technique are effected through the use of different scan geometries. Systems are presently available that are capable of linear, circular, elliptical, and hypocycloidal scans. In addition, multiple cassette systems exist with the capability of imaging several planes simultaneously. However, none of these systems exploit the full potential of body-section radiography hinted at by des Plantes; namely, sufficient information is projected in a single-patient scan to reconstruct all subject planes, that is, to produce a complete three-dimensional reconstruction.

Such an imaging technique which produces a three-dimensional reconstruction has been devised through

Manuscript received June 18, 1971; revised August 16, 1971. This work was supported by the National Institute of General Medical Sciences under Inter Agency Agreement Number NORD 012869-0190.

The author is with the Applied Physics Laboratory, Johns Hopkins University, Baltimore, Md.

Authorized licensed use limited to: Reprints Desk. Downloaded on February 12,2020 at 23:03:54 UTC from IEEE Xplore. Restrictions apply.

Dentsply Sirona Inc. – Exhibit 1029

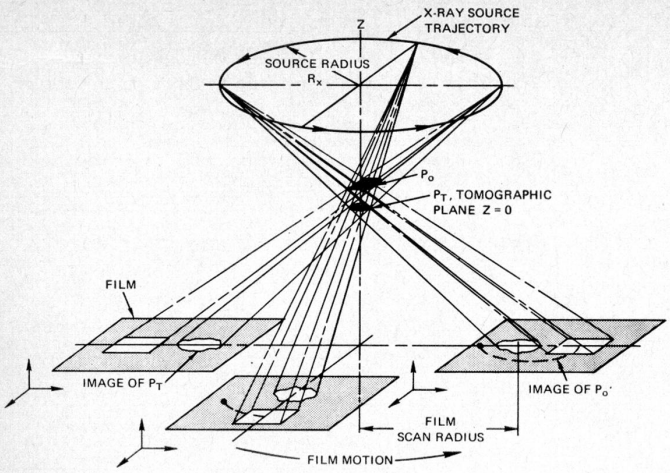


Fig. 1. Circular tomography.

a generalization of circular tomography. This work resulted in the development of a prototype three-dimensional image projector presently at Johns Hopkins Hospital, Baltimore, Md., for clinical evaluation. This paper contains an explanation of the underlying concept, summarizes results, and indicates extensions of the three-dimensional imaging technique into other biomedical disciplines.

II. Tomography

The geometrical concepts underlying all tomographic imaging systems are shown in Fig. 1. An X-ray point source and a film cassette are scanned through a trajectory constrained to image one subject plane (i.e., the tomographic plane) at the same location on the film. As the scan progresses, the image of the tomographic plane is continuously reinforced, while the remaining subject planes are blurred by the scanning motion. The effectiveness with which a tomographic system forms an image is measured by the degree of blurring incurred by the unwanted planes. Quantitatively, the blurring characteristic is difficult to specify in the spatial coordinate domain. However, analysis in the spatial frequency domain provides considerable insight into tomography, and also provides a completely general means of evaluating and comparing tomographic systems.

It is instructive at this point to make a direct comparison between conventional radiography and tomography. To eliminate nonessential details from the following analysis, parallel ray illumination and constant magnification over the object volume will be assumed. The X-ray source (see Figs. 2 and 3) produces an incident intensity I_s for a time duration T, resulting in a total incident source exposure

$$E_s = I_s T. \tag{1}$$

The object chosen in Fig. 2(a) consists simply of two planes P_T and P_0, with transmission profiles $G_T(X, Y)$ and $G_0(X, Y)$, respectively. The film exposure produced in the conventional case is given by

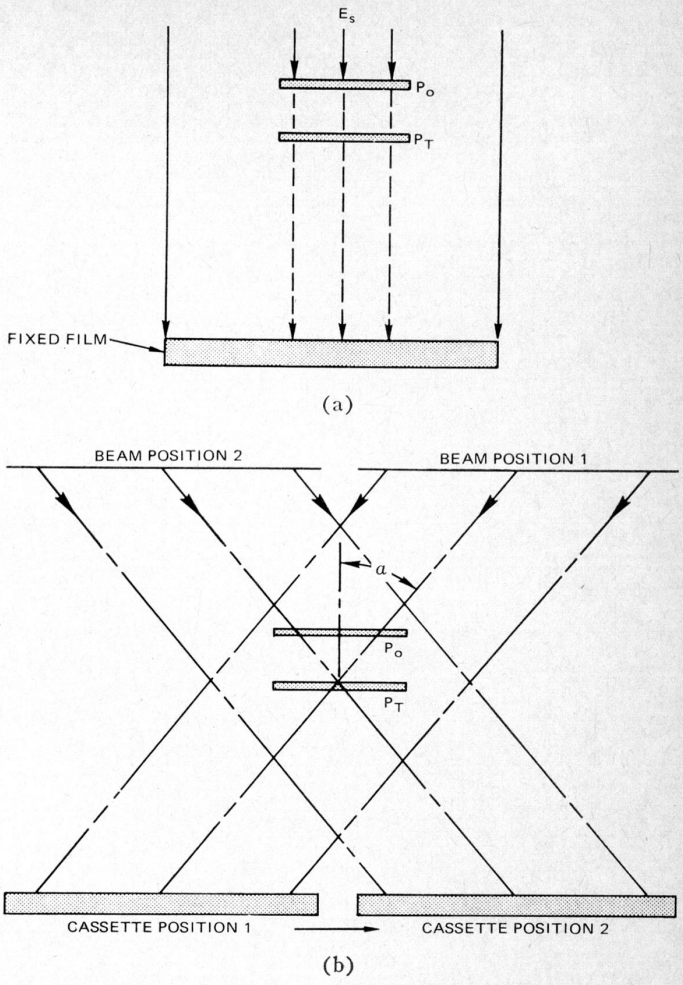


Fig. 2. (a) Conventional radiography $E(X, Y) = E_s G_0(X, Y) G_T(X, Y)$. (b) Linear-scan tomography.

$$E(X, Y) = E_s G_0(X, Y) G_T(X, Y). \tag{2}$$

A linear-scan tomographic system is shown in Fig. 2(b). In this case, the object is positioned so that P_T lies in the tomographic plane. Experience tells us that the image of P_T, as produced in Fig. 2(b), is superior to that produced in Fig. 2(a) insofar as visualization of structures lying in P_T is concerned. The quantitative reason for this provides the fundamental basis for tomography.

The relative motion of the plane images on the film is depicted in Fig. 3(a). By using simple geometry, it is shown that the image of plane P_T remains fixed, while the image of plane P_0 moves in a straight line during the scan. This suggests [Fig. 3(b)] that an equivalent conventional radiographic system can be defined to produce the same image as the tomogram. This is accomplished by using a synthesized object comprised of the tomographic plane P_T and an average plane $\overline{P_0}$ obtained by integrating the transmission profile of P_0

Authorized licensed use limited to: Reprints Desk. Downloaded on February 12,2020 at 23:03:54 UTC from IEEE Xplore. Restrictions apply.

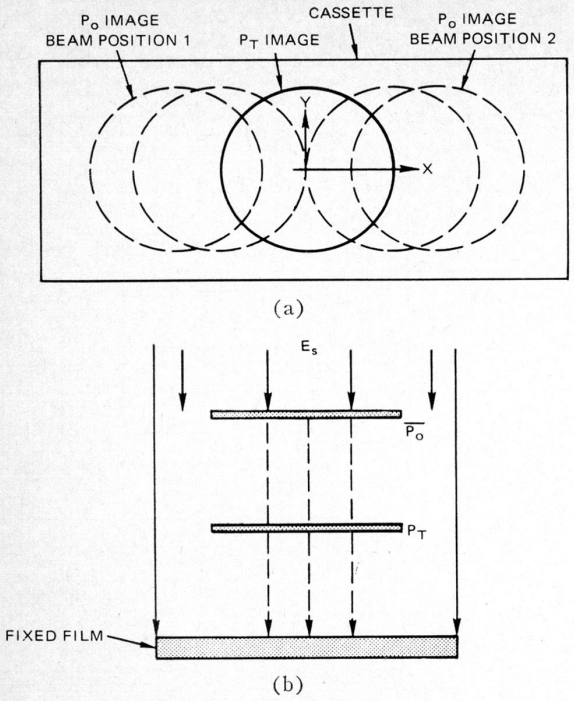


Fig. 3. Motion of P_0 image relative to P_T image. Equivalent radiograph $\overline{E}(X, Y) = E_s\overline{G_0}(X, Y)G_T(X, Y)$.

over the curve of relative motion (in this case, a straight line of length Δ) and normalizing. Hence, in Fig. 3(b) the transmission profile of $\overline{P_0}$ is given by

$$\overline{G_0}(X, Y) = \frac{\int_{X-\Delta/2}^{X+\Delta/2} G_0(X', Y)\, dX'}{\int_{X-\Delta/2}^{X+\Delta/2} dX'}. \quad (3)$$

Assuming the same total input exposure as Fig. 2(a), the resulting exposure is therefore

$$\overline{E}(X, Y) = E_s\overline{G_0}(X, Y)G_T(X, Y). \quad (4)$$

Rather than compare the systems through evaluation of (2) and (4) directly, much greater insight can be obtained through a comparison in the spatial frequency domain. In this regard, we define the general form for the spatial Fourier transform by

$$F(\omega_x, \omega_y) = \int_{-\infty}^{\infty}\int_{-\infty}^{\infty} G(X, Y)e^{-j(X\omega_x + Y\omega_y)}\, dX dY. \quad (5)$$

Equivalent expressions for $G_0(X, Y)$, $\overline{G_0}(X, Y)$, and $G_T(X, Y)$ can be obtained from this general form. Substituting (3) into (5) and changing the order of integration produces the result

$$\overline{F_0}(\omega_x, \omega_y) = \frac{\sin(\omega_x\Delta/2)}{(\omega_x\Delta/2)} F_0(\omega_x, \omega_y). \quad (6)$$

The fact that (6) has the form

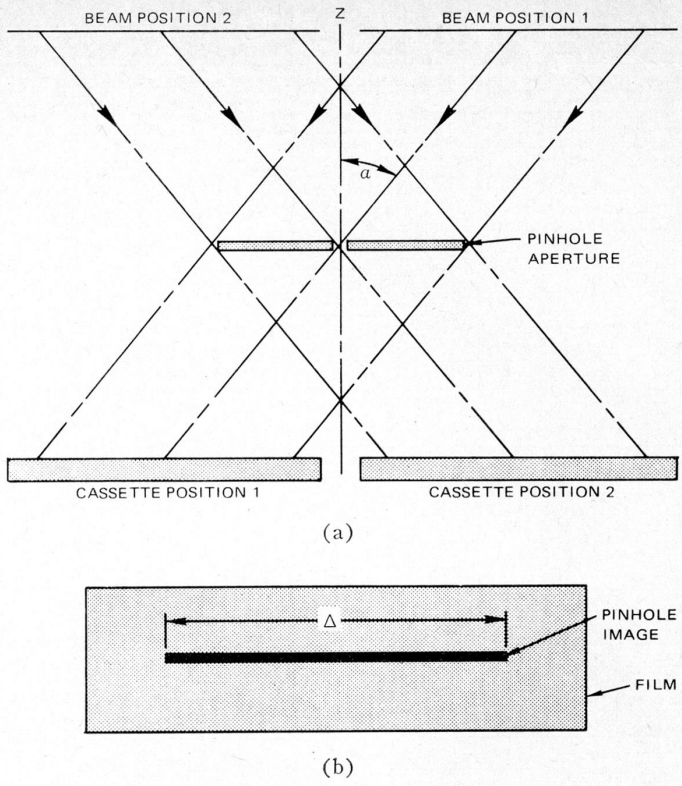


Fig. 4. (a) Impulse response measurements. (b) Impulse response, linear scan.

$$\overline{F_0}(\omega_x, \omega_y) = H(\omega_x, \omega_y)F_0(\omega_x, \omega_y) \quad (7)$$

suggests that the blurring process is, in fact, the result of a linear mathematical operation. Let us digress momentarily and investigate this possibility.

If linearity exists, then all input/output considerations will be determined through knowledge of the impulse–response function. A "delta-function" input is provided for the system in Fig. 4(a) by means of a radiopaque plane with a small pinhole located on the vertical axis. It is easily shown that this input produces a replica of the scan geometry on the film [Fig. 4(b)] with a Z dependent scaling factor. Furthermore, only the position of the response on the film, not its orientation or size, depends on the position of the delta function in the plane. The response is therefore invariant.

In the linear scan case, the impulse–response function is a line of length

$$\Delta = 2MZ \tan\alpha = KZ \quad (8)$$

where M is the X-ray magnification and α is the scan maximum half-angle. The Fourier transform of the impulse–response function yields the transfer function given by

$$H(\omega_x, \omega_y \mid Z) = \int_{-\Delta/2}^{\Delta/2} e^{-jX\omega_x}\, dX = \frac{\sin(\omega_x KZ/2)}{(\omega_x KZ/2)}. \quad (9)$$

Authorized licensed use limited to: Reprints Desk. Downloaded on February 12,2020 at 23:03:54 UTC from IEEE Xplore. Restrictions apply.

Hence, the linear systems analysis produces a result identical with the original derivation. We will proceed under the assumption that linearity exists.

Assuming unity incident exposure, the spectrum of $E(X, Y)$, given in (2), can be derived from the convolution form ([2], [3])

$$F(\omega_x, \omega_y) = (2\pi)^{-2} \int_{-\infty}^{\infty} \int_{-\infty}^{\infty} F_T(\xi, \eta) F_0(\omega_x - \xi, \omega_y - \eta)\, d\xi d\eta. \quad (10)$$

Also from (4), the spectrum of $\overline{E}(X, Y)$ is given by

$$\overline{F}(\omega_x, \omega_y) = (2\pi)^{-2} \int_{-\infty}^{\infty} \int_{-\infty}^{\infty} F_T(\xi, \eta) \overline{F_0}(\omega_x - \xi, \omega_y - \eta)\, d\xi d\eta. \quad (11)$$

Because of linearity, we can write for an arbitrary scan geometry

$$\overline{F_0}(\omega_x - \xi, \omega_y - \eta) = H(\omega_x - \xi, \omega_y - \eta \mid Z) F_0(\omega_x - \xi, \omega_y - \eta). \quad (12)$$

If the system is designed so that $H(\omega_x, \omega_y \mid Z)$ is a narrow low-pass filter, then

$$\overline{F_0}(\omega_x - \xi, \omega_y - \eta) \rightarrow (2\pi)^2 \delta(\omega_x - \xi) \delta(\omega_y - \eta) \quad (13)$$

and

$$\overline{F}(\omega_x, \omega_y) \rightarrow F_T(\omega_x, \omega_y) \quad (14)$$

and visualization is improved, as compared to (10).

Note that in the linear-scan case, frequency components normal to the scan direction are not attenuated by the scanning motion. This accounts for the comparatively poor images produced with this scan, as compared with more complicated scan geometries.

The above procedure can also be followed for a circular scan geometry. In this case, the impulse response is a circle whose radius is Z-axis dependent according to

$$a(Z) = MZ \tan \alpha = \frac{KZ}{2}. \quad (15)$$

The corresponding transfer function is given by

$$H(\omega_x, \omega_y \mid Z) = \frac{\oint e^{-j(X\omega_x + Y\omega_y)}\, ds}{\oint ds} = J_0[a(Z)\omega_r] \quad (16)$$

where $\oint$ denotes integration over the circle, $\omega_r^2 = \omega_x^2 + \omega_y^2$, and J_0 is a zero-order Bessel function.

It should be apparent that the above analysis can be generalized to suit any geometry. To summarize, we have shown the following to be true.

1) The blurring of unwanted planes is basically a linear filtering process.

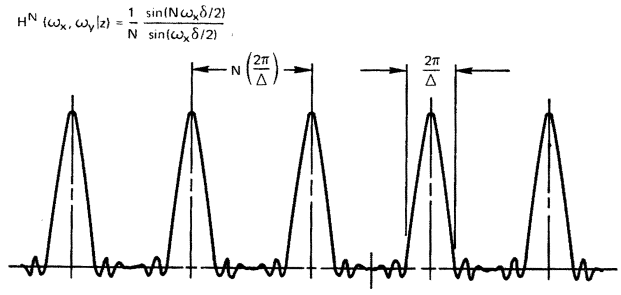


Fig. 5. N sample transfer function, linear scan.

2) The system's impulse response is a scaled replica of the scan geometry.

3) The size of the impulse response is Z-axis dependent. The limiting situations result in the transfer functions

$$H(\omega_x, \omega_y \mid 0) = 1, \qquad H(\omega_x, \omega_y \mid Z_{\text{large}}) = \delta(\omega_x)\delta(\omega_y).$$

4) The transfer function is a direct quantitative measure of the system's ability to blur unwanted planes and provides a valid means of comparing systems. It also provides a means of evaluating the effectiveness of a particular scan geometry *a priori* without having to resort to actual measurement.

The transfer function for linear and circular scans are tabulated in [4].

III. N-Sample Tomography

The previous section contains the derivations of transfer functions for linear and circular scans, assuming the illuminating radiation is continuously integrated. It is also instructive to investigate sampled systems where a series of N images, uniformly distributed along the trajectory arc length, are projected onto the integrating film. The N sample case also lends itself to linear systems analyses.

For a linear geometry, the impulse response is simply a series of N infinitesimal points. The corresponding transfer function computed by the sum

$$H^N(\omega_x, \omega_y \mid Z) = \frac{1}{N}\left[1 + \sum_{n=1}^{(N-1)/2} (e^{-jn\delta\omega_x} + e^{jn\delta\omega_x})\right] \quad (17)$$

reduces to

$$H^N(\omega_x, \omega_y \mid Z) = \frac{1}{N} \frac{\sin N\left(\frac{\delta\omega_x}{2}\right)}{\sin\left(\frac{\delta\omega_x}{2}\right)}. \quad (18)$$

The results of sampling are quite predictable (Fig. 5). The transfer function becomes a series of peaks occurring at harmonics of the sampling frequency. That is,

Authorized licensed use limited to: Reprints Desk. Downloaded on February 12,2020 at 23:03:54 UTC from IEEE Xplore. Restrictions apply.

for

$$\omega_q = q\left(\frac{2\pi}{\delta}\right), \qquad q = 0 \pm 1 \pm 2 \cdots. \tag{19}$$

However, the width of the peaks is still determined by the total scan length

$$\omega_\Delta = \frac{2\pi}{N\delta} = \frac{2\pi}{\Delta} \tag{20}$$

as in the continuous case.

For the circular scan, the samples are distributed uniformly around the circumference, resulting in an angular periodicity. Here we perform the summation

$$H^N(\omega_x, \omega_y \mid Z) = \frac{1}{N}\sum_{n=1}^{N} e^{-j(X_n\omega_x + Y_n\omega_y)}. \tag{21}$$

Making the substitutions

$$\begin{aligned} X_n &= a(z)\cos n\phi, & \omega_x &= \omega_r \cos\Psi \\ Y_n &= a(z)\sin n\phi, & \omega_y &= \omega_r \sin\Psi \end{aligned} \tag{22}$$

(21) reduces to ([5])

$$H^N(\omega_r, \Psi \mid Z) = J_0[a(z)\omega_r] + \frac{4}{N}\sum_{p=1}^{\infty} J_{(pN)}[a(z)\omega_r]\cos\left(\frac{N+2}{2}\pi p - N\Psi p\right). \tag{23}$$

The sampled transfer function contains the transfer function for the continuous case as its first term, but also contains higher order Bessel functions. The importance of the higher order terms is minimal near the origin. For large values of the argument, however, these terms do become significant. This spectrum does not exhibit true radial harmonics, but does possess an almost-periodic ring structure due to the occurrence of the J_{pN} maxima. The angular periodicity is evident in that J_{pN} is modulated by a cosine function which goes through pN cycles as Ψ goes from 0 to 2π. The argument at which the first $J_{pN}(\rho = \rho_N)$ peak occurs as a function of pN is tabulated in [4].

The previous discussion now raises an obvious question, namely, how many samples are required to effect the same blurring as in the continuous case? If we assume the plane P_0 is band-limited, then the relevant theorems of sampling theory may be applied. In the linear case, if

$$F_0(\omega_x, \omega_y) = 0, \qquad |\omega_x| > \omega_0 \tag{24}$$

then we require a sampling interval on the film of

$$\delta = \frac{\Delta}{N} \leq \frac{1}{2}\left(\frac{2\pi}{\omega_0}\right). \tag{25}$$

Using (8) we have

$$N \geq \frac{2MZ\tan\alpha}{\pi}\omega_0. \tag{26}$$

In the circular case, assume the spectrum of plane P_0 has the property

$$F(\omega_x, \omega_y) = 0, \qquad \omega_x^2 + \omega_y^2 \geq \omega_0^2. \tag{27}$$

To produce the same blurring as conventional circular tomography we want to select N such that the peak of (J_N), the first higher order Bessel function (21), falls outside the band. Now the argument of $J_N(\rho)$ at which the first peak occurs ($\rho = \rho_N$) is a function of N. However, for a given ω_0, we can always select an N such that

$$\rho_N > 2a(z)\omega_0 = MZ\tan\alpha\omega_0. \tag{28}$$

The tables in [4] can be used to determine N such that (28) is satisfied.

The previous equations show that the transfer function generated by the scanning motion is Z-axis dependent. They also show that for any Z, we can always achieve the same degree of filtering as conventional tomography if N is chosen sufficiently large. In a clinical situation, however, patient time and dosage considerations limit N to some tens of views. This constraint produces a filtering process which is identical with conventional tomography for planes near the tomographic plane, but which is less effective for more distant planes.

Consider momentarily that a distant plane P_0 has a well-defined cutoff frequency, and that a linear scan is being used. The number of peaks spaced at the spatial sampling frequency within bandwidth $2\omega_0$ is given by the greatest integer in

$$P = \frac{2\omega_0}{N}\frac{\Delta}{2\pi}. \tag{29}$$

Therefore, the total bandwidth of the image [using (20)] is

$$W = P\cdot\omega_\Delta = \frac{2\omega_0}{N}. \tag{30}$$

Equation (30) states that the scanning process reduces the frequency content of each object plane (distant from P_T) by the factor of $1/N$. Equivalent expressions can of course be derived for all other scan geometries. While the total blurring effect produced is not as great as conventional tomography, it typically approaches conventional tomography for reasonable values of N, e.g., $N = 20$.

IV. Three-Dimensional Imaging

In forming a tomographic image by the process described in the previous section, it is not essential to integrate directly onto a single film. For instance, the different views could in principle be recorded on N separate films, and the data summed therefrom to form the tomographic plane. There are many ways to perform the indicated summation: for example, digitization followed by computer summation, an N-channel flying

Authorized licensed use limited to: Reprints Desk. Downloaded on February 12,2020 at 23:03:54 UTC from IEEE Xplore. Restrictions apply.

spot scanner, a sequence of N contact prints, superposition of N projected images, etc., to name only a few. Further, the record need not be film. Video disk recorders could also be used as an alternate means, although certain technical problems resulting from distortion occur with this approach.

The significance of obtaining N separate data records is that it affords the opportunity not just to produce a single plane, but to produce all object planes. That is, sufficient information is recorded by this method to produce a three-dimensional image. The reasoning for these statements is as follows. In conventional tomography, the tomographic plane can be adjusted simply by changing the scanning radius of the film (see Fig. 1). This change shifts the system fulcrum along the Z axis and results in a new tomographic plane. No other changes are required. Moving the fulcrum point, however, amounts simply to displacing the family of impulse–response functions (recalling their Z dependence) and their corresponding transfer functions along the Z axis. Hence, the identical input data is used to reconstruct an entirely different plane. The same arguments also pertain to the N sample case. Here, direct imaging on a single film produces the tomographic image of a plane passing through the fulcrum. If the film radius is changed, resulting in a new fulcrum point, a new tomographic plane is formed from the same input data.

The advantage of recording on N separate radiographs now becomes clear. To reconstruct the central tomographic plane, one sums the data off the radiographs (say by N sequential contact prints) being sure the image of the fulcrum point is registered in all views. To obtain a new plane (parallel to the scan plane), one simply displaces the radiographs radially until the new fulcrum point is registered in all views and a new summation is performed. Notice that the plane of reconstruction can be varied continuously.

Hence, the problem of reconstructing an arbitrary object plane is simply one of summing the data on the N radiographs in some unique way. It is of particular interest to note that this same data can be utilized to reconstruct tilted planes, i.e., ones not parallel to the scan plane. This capability is accomplished by first projecting each radiograph parallel to the plane of interest, and then performing a summation. Therefore, the N-input radiographs afford a means of observing a structure within the three-dimensional object from any angle. Three-dimensional images can be produced from a generalized scan geometry provided, of course, the summation arithmetic is properly performed.

V. Three-Dimensional Recording and Projecting System

An optical summation technique which produces a real three-dimensional image has been devised and fabricated. The image is formed in a 7-in diameter spherical

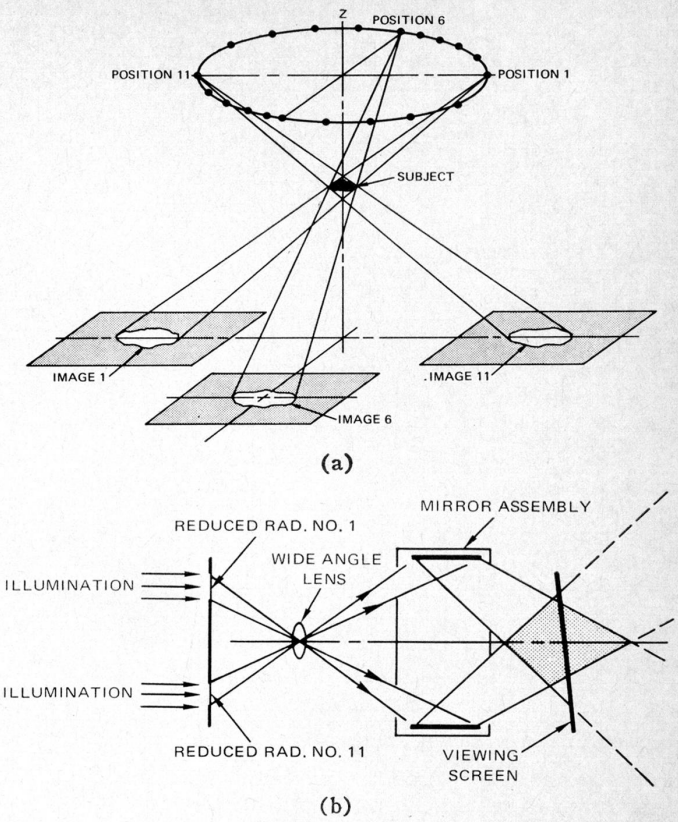


Fig. 6. (a) Circular scan, N views. (b) Three-dimensional projector geometry.

display volume, and is observed by means of a movable viewing screen. The image on the screen corresponds to a planar cross section of the subject, and is continuously variable throughout the display volume. As an input to the system, a set of 20 radiographs are recorded from a circular scan geometry (uniform separation) as shown in Fig. 6(a). These radiographs are photoreduced onto a single film (described below) and reprojected into the display volume as shown in Fig. 6(b). The reprojection is accomplished by means of a wide-angle lens and a mirror assembly whose geometry duplicates the X-ray system geometry. Placing a viewing screen in the display volume causes the individual images to sum and produce the tomographic plane corresponding to the screen position. Moving the screen to a different position causes the input to sum differently and form a new image. Hence, the "way" the data are summed to compute a particular tomographic plane, including tilted planes, is determined automatically.

A cutaway view of the projector is shown in Fig. 7. The basic projector structure is a precision 20-sided regular polygon, upon which the mirrors are fixed, mounted on a cast-aluminum cylinder. The cylinder serves as a means of locating the mirror planes, lens plane, and film plane with great precision (angular tolerance 0.01°, linear tolerance 0.0002 in). The input film is held on a glass plate and is located precisely by

Authorized licensed use limited to: Reprints Desk. Downloaded on February 12,2020 at 23:03:54 UTC from IEEE Xplore. Restrictions apply.

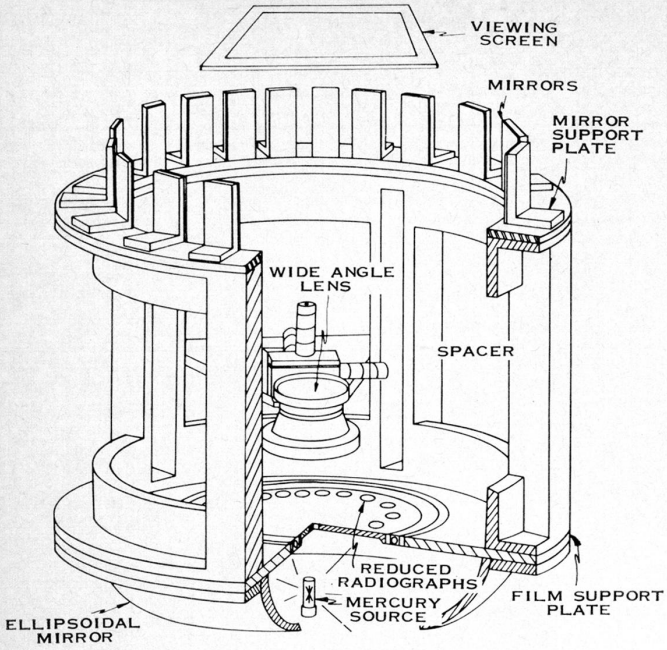


Fig. 7. Three-dimensional projector, cutaway view.

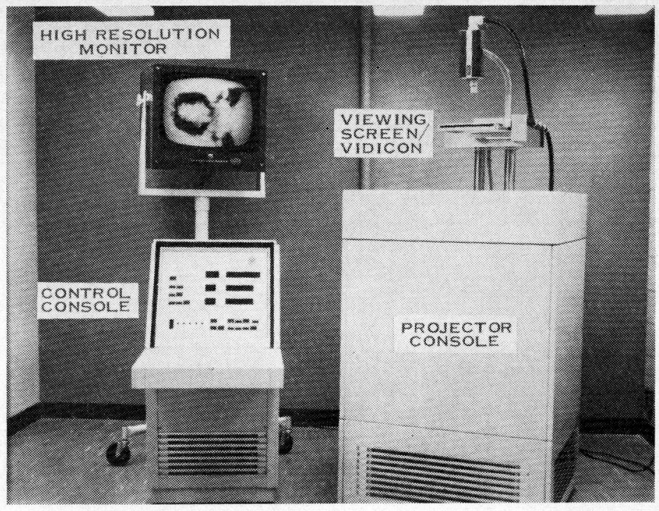


Fig. 8. Three-dimensional projection system.

means of reference dowels. Each of the reduced radiographs thereon is imaged in the display volume by first reflecting off one of the mirrors. The lens is a Schneider Super Angulon 240 mm wide-angle lens, and is held by a high-precision three-axis translator. Image magnification has been chosen to produce a true-sized three-dimentional image. A 100-W Hg lamp and ellipsoidal mirror mounted underneath the cylinder serve as an illumination source.

The viewing system consists of a high-resolution vidicon camera and viewing screen which are remotely scanned through the display volume (Fig. 8). The control console contains viewing-screen position controls, camera-control electronics, and screen-coordinate readouts obtained from shaft-angle encoders.

Input radiographs for the three-dimensional projector are obtained by means of a camera attached to a standard Polytome. The procedure is shown in Fig. 9(a) and (b). The Polytome drive mechanism has been modified to step through 20 fixed locations with high precision. At each position, the X-ray source is pulsed, forming an image on the phosphor screen shown in Fig. 9(a). The screen is followed by an $F/0.87$ Super Farron reduction lens (4/1), and an RCA type C-33050 electrostatic image intensifier which is coupled to a 70 mm film via fiber optics. The 70 mm film is magazine-loaded in a high-precision film-transport mechanism.

When a scan is completed, the 70 mm filmstrip is processed automatically and loaded in the film transport shown on the intermediate projector [Fig. 9(b)]. This intermediate projector is mounted temporarily on top of the three-dimensional projector, and has a projection screen located in the central tomographic plane of the display volume. The recording process is initiated by the intermediate projector which automatically se-

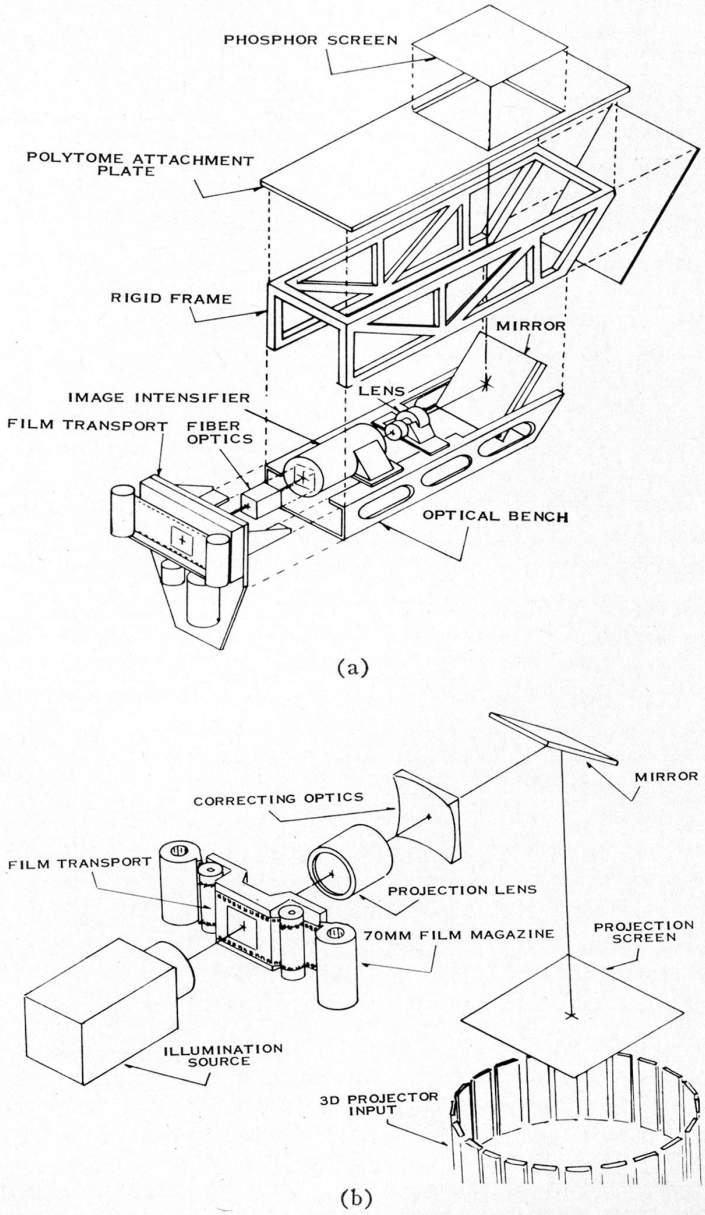
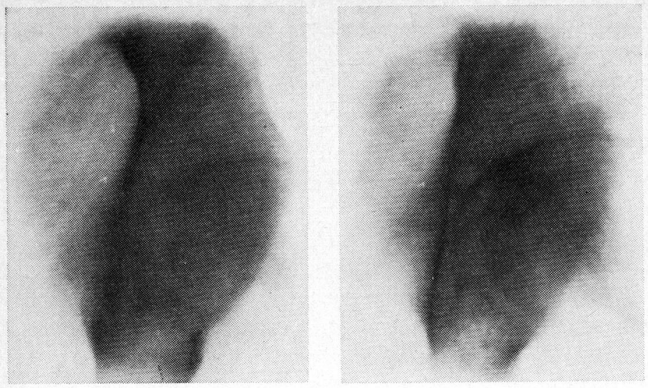


Fig. 9. (a) Polytome camera. (b) Intermediate projector.

Authorized licensed use limited to: Reprints Desk. Downloaded on February 12,2020 at 23:03:54 UTC from IEEE Xplore. Restrictions apply.

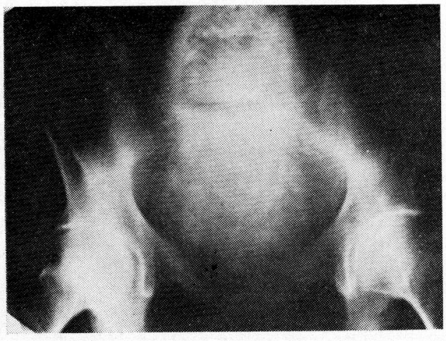


(a) (b)

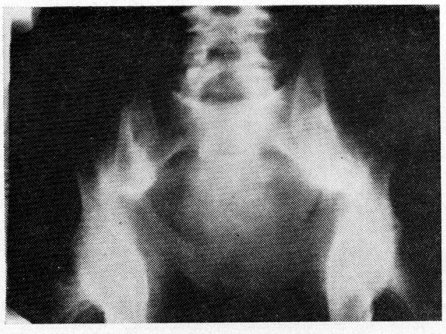


(c)

Fig. 10. Hip sections. Subject—phantom, image-screen magnification 1.2/1.

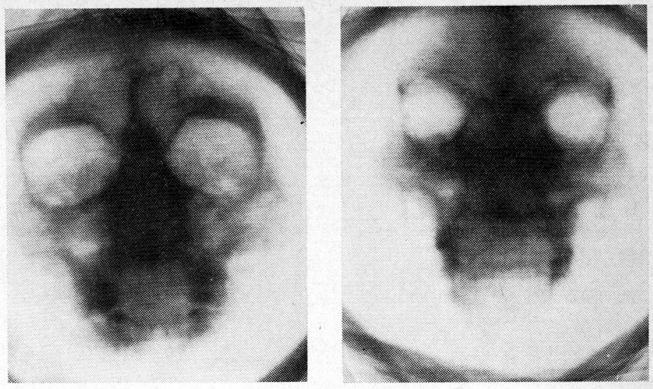


(a)



(b)

Fig. 11. Pelvic section. Subject—phantom, image-screen magnification 0.435/1.



(a) (b)

Fig. 12. Skull sections. Subject—phantom, image-screen magnification 1.2/1.

que ıces through the 20 radiographs, magnifying them back to their original size on the projection screen. Prior to this, a special cassette has been mounted in the film plane of the three-dimensional projector. This cassette uses a rotating shutter to scan the film synchronously with the film transport. This results in the 20 radiographs being recorded on a single film. The final film is processed and placed back in the projector for display. The process just described has the considerable advantage of being self-correcting. That is, first-order misalignments of the lens and mirrors are compensated because the projected image uses the same path as the recorded image. All that is required is that the images produced by the intermediate projector be positioned exactly relative to one another.

VI. Results

Initial use of the projector has included models, dried skulls [6] and [7], phantoms, and animals. Results have been obtained on a total of approximately 50 different subjects, and results are very encouraging. Resolution on the order of 2 line pairs/mm have been obtained in the display volume. (Note that the camera described above was not used for these tests as it was not yet completed. Instead, a conventional double-screen film cassette was used.)

A number of interesting results are shown in Figs. 10–12. Extensions and applications into all areas of radiography should be readily apparent. Note that while the display volume is fixed in diameter, it is possible to present magnified, or demagnified images with full resolution by changing the scale of the input data.

VII. Conclusions

The production of a three-dimensional X-ray image has been a goal long sought after by radiologists. Existing stereoscopic techniques, while extremely valuable, do not allow the radiologist to see behind opacities or to make physical measurements. Recently, holographic techniques have been devised based on N separate views for producing a virtual image of the entire object volume. These techniques, their difficulty notwithstanding,

Authorized licensed use limited to: Reprints Desk. Downloaded on February 12,2020 at 23:03:54 UTC from IEEE Xplore. Restrictions apply.

do not attack the fundamental problem, that is, suppression of nonessential data in the observed image.

The method of integrated images described in this paper produces a real three-dimensional image which is observable on a plane-by-plane basis. The most significant properties of this image are that each observed plane is produced with maximum clarity (i.e., they are "tomographic"), the fact that the image is continuous in all directions, and finally, the truly three-dimensional characteristic of being able to observe behind opacities. This sort of presentation is ideal for diagnostic radiography.

The prototype system described herein has been developed as an extension of circular tomography. The technique, of course, can be generalized to linear, elliptical, or hypocycloidal geometries. The same relative quality would presumably result, as it occurs in conventional tomography. A further generalization would be to move the source to random locations over a hemisphere. To be sure, there are varying degrees of difficulty involved in implementing the different optical-projector systems. In this sense the circular geometry is quite simple.

The utilization of N-fixed high-resolution sources, rather than a single scanning source while speeding up the normal clinical procedure, also introduces the possibility of recording time-varying events in three dimensions.

Alternate methods of recording and handling input data can be utilized depending on the ultimate resolution requirements. For instance, a vidicon pickup-video disk storage memory could replace the film in the Polytome camera system. This data could be played directly into the projector by using a large-screen precision monitor in the present film plane. To date, techniques of this sort are limited by various distortions to low-resolution applications.

In a broader sense, the three-dimensional imaging technique described in this paper is not restricted to radiography. For instance, a series of N electron micrographs, each corresponding to a different view, can in principle be projected in the same manner as above to produce a three-dimensional image of a structure magnified by 10^5.

Finally, it should be noted that in the field of nuclear medicine, with a radioisotopic source internal to the structure, an optical system has been devised [8] to produce a three-dimensional image of the source distribution.

Acknowledgment

The author wishes to thank Dr. J. B. Garrison of the Applied Physics Laboratory, and Dr. R. J. Johns of the Johns Hopkins School of Medicine for their substantial technical contributions to this program. He also wishes to thank Dr. F. T. McClure, Dr. R. H. Morgan, Dr. J. T. Massey, and Dr. W. H. Guier, all of whose consultation and collective interest proved very valuable during the course of this work. Technical assistance was provided by R. A. Meyer, G. S. Bittings, J. E. Marrow, and C. R. Flick of APL, and Mrs. Carol Digel of the Johns Hopkins Hospital.

References

[1] Ziedses des Plantes, "Eine neue methods zur differenzierung in der roentgenographie," *Acta Radiol.*, vol. 13, 182–192, 1932.
[2] A. Papoulis, *The Fourier Integral and its Applications*. New York: McGraw-Hill, 1962.
[3] J. W. Goodman, *Introduction to Fourier Optics*. New York: McGraw-Hill, 1968.
[4] Jahnke and Emde, *Tables of Functions*. Stuttgart, Germany: Teubner, 1943.
[5] H. F. Davis, *Fourier Series and Orthogonal Functions*. Boston, Mass.: Allyn and Bacon, 1963.
[6] D. G. Grant *et al.*, "Three-dimensional roentgenography," *Amer. J. Roentgenol., Radium Ther., Nucl. Med.*, vol. CV, Apr. 1969.
[7] D. G. Grant *et al.*, "Three-dimensional X-ray imaging," in *Proc. 7th Nat. Biomed. Sci. Instrumentation Symp.*, May 1969.
[8] P. V. Harper, "The three-dimensional reconstruction of isotope distributions," in *Fundamental Problems in Scanning*. Springfield, Ill.: Charles C Thomas, 1968.

Authorized licensed use limited to: Reprints Desk. Downloaded on February 12,2020 at 23:03:54 UTC from IEEE Xplore. Restrictions apply.